Analyst

ROYAL SOCIETY OF CHEMISTRY

PAPER

View Article Online
View Journal | View Issue



Cite this: *Analyst*, 2022, **147**, 1716

# An ultrasensitive electrochemiluminescence biosensor for the detection of total bacterial count in environmental and biological samples based on a novel sulfur quantum dot luminophore†

Xiaobin Wang, Yuqing Zhao, Qing Hua, Jiaojiao Lu, Feiyan Tang, Wenjie Sun, Feng Luan, Xuming Zhuang * and Chunyuan Tian*

In this paper, the electrochemiluminescence (ECL) of sulfur quantum dots (SQDs) in a potassium persulfate cathodic co-reactant was studied. Based on the selective quenching of the ECL emission from the SQDs by β-nicotinamide adenine dinucleotide (NADH), an ultrasensitive ECL biosensor with NADH as an important parameter was established for the highly sensitive and selective detection of total bacterial count (TBC). A linear response between the ECL intensity and the NADH concentration in the range of 1 pM to 10 μM was obtained, thus achieving a detection limit of 1 pM. As the content of NADH in cells is positively correlated with the TBC, a sensor has been successfully applied to detect the TBC in actual water samples with a good recovery rate of $10^3$–$10^7$ CFU $mL^{-1}$. This study provides a green and feasible method for TBC detection in the environment.

Received 23rd January 2022,
Accepted 10th March 2022

DOI: 10.1039/d2an00153e

rsc.li/analyst



## Introduction

The total bacterial count (TBC), which has a direct and huge impact on human health, is an internationally recognized sanitary bacteriological indicator of drinking water and food safety and fecal pollution. Therefore, it is important to develop novel methods for the sensitive and selective detection of the TBC in human production and life, which could lead to spoilage of food and animal and plant diseases. It could provide a scientific basis for health management in terms of food hygiene and safety,[1–3] allow for the prevention and control of infectious diseases and food poisoning, effectively prevent or reduce the occurrence of food poisoning and zoonotic diseases, and protect people's health in terms of disease treatment.[4–6] Moreover, the sensitive and selective detection of the TBC is of great significance for improving environmental sanitation and living standards. Common detection methods include the traditional plate counting method (PCM),[7,8] the turbidimetric method,[9] and the emerging polymerase chain reaction[10,11] and enzyme-linked immune-sorbent assay.[12,13] In recent years, some substances in cells have been used as indicators of the TBC, such as adenosine triphosphate and β-nicotinamide adenine dinucleotide (NADH). Herein, NADH was used as an important parameter to measure the TBC.

NADH, which is universally present in living cells, plays an indispensable role in maintaining cell growth, differentiation, energy metabolism, protection, *etc.*, although its main role is to participate in intracellular redox reactions, such as the Krebs cycle.[14–16] A method of releasing NADH that shows a strong quantitative relationship with the TBC within a certain range was developed to lyse *Escherichia coli* (*E. coli*). Common methods for detecting NADH include fluorescence,[17,18] enzymatic cycling,[19,20] electrochemistry,[21,22] and chromatography.[23,24] Although many methods for detecting NADH have shown satisfactory results, selecting appropriate technology for the establishment of a high-sensitivity and high-accuracy sensing platform has been a challenge.

Electrochemiluminescence (ECL) is a specific luminescence reaction initiated electrochemically on the electrode surface, and it shows both electrochemical and chemiluminescence features. ECL has been widely used in biological science for immunoassays, food analyses and environmental monitoring due to its high speed, high sensitivity and simple equipment.[25,26] In recent years, an increasing number of quantum dots have been observed and attracted wide attention. Although traditional quantum dots can be used as ECL emitters due to their high sensitivity and good optical properties, their application is limited by potential heavy metal contamination.[27,28] Compared with these conventional quantum dots, inexpensive, easy to prepare, low toxicity and environmentally friendly pure-element quantum dots must be developed.

*College of Chemistry and Chemical Engineering, Yantai University, Yantai 264005, China. E-mail: xmzhuang@iccas.ac.cn, cytian@ytu.edu.cn*

† Electronic supplementary information (ESI) available. See DOI: https://doi.org/10.1039/d2an00153e

In recent years, sulfur quantum dots (SQDs) have been developed as a new type of pure elemental quantum dot material. To date, few studies and applications have focused on the ECL performance of SQDs, which is worthy of further discussion. Compared to other quantum dots, especially traditional heavy metal quantum dots, SQDs are safer for biological samples and more environmentally friendly. Because of the low biotoxicity and high biocompatibility of SQDs, they have gradually attracted the attention of researchers and received extensive attention. Many researchers have begun to study this effective and convenient synthesis method. Shen *et al.* developed an "assembly fission" synthesis mechanism using polyethylene glycol-400 (PEG-400) as a passivator.[29] Wang and colleagues developed a hydrogen peroxide ($H_2O_2$)-assisted top-down method to synthesize SQDs based on Shen's method.[30] To date, many applications have focused on using good optical properties to study fluorescent probes to detect heavy metal ions, although few reports have investigated the ECL performance of SQDs.

In this work, the ECL performance of SQDs was extensively studied at a scanning potential of −2 to 0 V. Furthermore, the mechanism of the sensor is described systematically, as shown in Scheme S1.† Based on the positive correlation between the NADH content and the TBC, a new type of ultrasensitive ECL sensor was developed for the detection of the TBC, and it is characterized by low cost, fast detection speed and high selectivity. The sensor prepared by this method detected the TBC in real samples, such as lake water, river water and mouse serum. The method of establishing the sensor provided a good example of combining SQDs with ECL technology and represented a novel idea for effectively detecting the TBC, which is of great significance for improving the quality of the environment and the standard of life.

## Experimental section

### Reagents

Sublimed sulfur powder, PEG-400, sodium hydroxide (NaOH), Triton X-100, urea and glucose were purchased from Shanghai Aladdin Biochemical Technology Co., Ltd (Shanghai, China). $H_2O_2$ (v/v, 30%) and potassium persulfate ($K_2S_2O_8$) were obtained from Sinopharm Chemical Reagent Co., Ltd (Tianjin, China). Dopamine (DA), L-ascorbic acid (AA) and uric acid (UA) were purchased from Sigma-Aldrich (Shanghai, China). *E. coli* were obtained from Guang Rui Biological Technology Co., Ltd (Shanghai, China). All solutions involved in this experiment were prepared with ultrapure water (18.25 MΩ cm).

### Instrumentation

High-resolution transmission electron microscopy (HR-TEM) images were obtained using a JEM-2100F transmission electron microscope at an accelerating voltage of 200 kV (JEOL Ltd, Japan). A Nicolet 5700 Fourier transform infrared (FT-IR) spectrometer (Thermo Electron Corporation, USA) was used to obtain the FT-IR spectra. Ultraviolet-visible absorption spectroscopy (UV-vis) was performed using an A560 ultraviolet-visible spectrometer (AOE Instruments, Shanghai) at wavelength intervals of 2 nm. X-ray photoelectron spectroscopy (XPS) was performed using a Thermo ESCALAB-250 (Thermo Fisher Scientific, USA). The fluorescence emission spectrum was obtained using an F-4700 fluorescence spectrophotometer (HITACHI, Japan). The ECL measurement was conducted using an MPI-E ECL analyzer from Xi'an Remax Analysis Instrument Co. Ltd (China). A three-electrode system was used in the experiment: a glassy carbon electrode (GCE), Ag–AgCl (sat. KCl) electrode and platinum wire electrode were used as the working electrode, reference electrode and auxiliary electrode, respectively, in the three-electrode system.

### Synthesis of SQDs

SQDs were prepared according to a top-down approach, as previously reported.[30] Briefly, 1.4 g of sublimed sulfur powder was weighed into a round-bottom flask, and then 3 mL of PEG-400 was added. The prepared NaOH solution (0.08 g $mL^{-1}$, 50 mL) was poured into a round bottom flask, stirred and heated in an oil bath at 70 °C for 24 h. After the color changed from bright yellow to orange-red, $H_2O_2$ (about 7.5%) was added to it for etching. The synthesized SQDs were stored at 4 °C for further experiments.

### Construction of the ECL sensor

In simple terms, the electrode modified with SQDs was obtained by dropping 5 μL of SQDs onto the polished GCE surface. NADH solutions of different concentrations were prepared with PBS buffer (0.1 M, pH = 7.4). In this system, the ECL sensor was fabricated with 50 mM $K_2S_2O_8$ PBS buffer (0.1 M, pH = 7.4) as a co-reactant. Scheme S1† shows the fabrication procedure of the ECL sensor. SQDs on the electrode surface reacted with the $K_2S_2O_8$ co-reactant to produce a strong and stable ECL signal. When NADH appeared in the co-reactants, the reaction between the SQDs and $K_2S_2O_8$ was inhibited and the ECL signal was quenched. In this way, the ECL sensor was obtained.

### Culture of *E. coli* strains and collection of NADH

*E. coli* was provided by the Coastal Zone Research Institute of the Chinese Academy of Sciences. *E. coli* single colonies were cultured in nutrient broth medium and incubated under constant temperature oscillation at 37 °C and 150 rpm for 12 h to the logarithmic growth stage, which was used as the initial bacterial liquid. One milliliter of initial bacterial liquid was inoculated into 100 mL nutrient broth medium for culture for 12 h at a ratio of 1 : 100, and set aside for use.

After culturing for 12 h, 3 mL of the bacterial suspension was processed by centrifugation at 10 000 rpm for 10 min at 4 °C, and the wet bacteria were collected and used as initial bacterial cells. Lysis buffer extraction was combined with the ultrasonic method, and 3 mL aseptic lysis solution (100 mM Tris–HCl, 10 mM EDTA, and 0.05% Triton X-100, pH = 8.0) was used to reconstitute the collected bacterial cells. Magnetic oscillation was performed to evenly mix the samples, and then

they were ultrasonically broken on ice. The ultrasound time for each sample was 10 s, with an interval of 10 s, and ultrasonication was performed for 30 min at a power of 400 W.

### Application of the ECL sensor in detecting the TBC

The bacterial suspension was diluted to $10^7$ CFU mL$^{-1}$, $10^6$ CFU mL$^{-1}$, $10^5$ CFU mL$^{-1}$, $10^4$ CFU mL$^{-1}$ and $10^3$ CFU mL$^{-1}$ (obtained by the plate counting method). The selected lysate combined with the ultrasonic extraction method was used to extract intracellular NADH from the bacteria for ECL determination. The relationship curves between the ECL intensity and bacterial suspensions were then established.

### Real sample analyses

Real samples were obtained from two sources. First, field samples were collected from nearby water sources to detect the TBC in tap water, river water, and lake water to evaluate the water quality; and second, samples were collected from mouse serum (from Yantai University College of Life Sciences). After the above-collected samples underwent the same treatment as *E. coli*, the TBC was detected using the sensor, and a certain number of *E. coli* were added to the real sample to perform a standard addition recovery experiment.

## Results and discussion

### Characterization of SQDs

The microstructure, functional groups and optical properties of the SQDs were investigated, and the morphology and size of the SQDs were studied by HR-TEM. The appearance of the SQDs was spherical, and they showed good dispersibility, and almost no particle aggregation (Fig. 1A). The inset of Fig. 1A shows the particle size distribution of the SQDs, which indicates that the particle size of most SQDs was less than 5 nm and primarily concentrated at 3–4 nm, and this analysis also provided proof of the successful preparation of SQDs. To further clarify the possible interaction between PEG-400 and SQDs, FT-IR spectroscopy was used for related investigations (Fig. 1B). In the FT-IR spectra of pure PEG-400 and SQDs, characteristic PEG-400 peaks of the C–H stretching vibration, C–H bending vibration and O–H stretching vibration were located at 2870, 1452 and 946 cm$^{-1}$, respectively. A comparison of PEG-400 with the SQDs showed that the peak intensity of PEG-400 at 1650 cm$^{-1}$ was slightly lower than that of the SQDs; moreover, a broad peak appeared near 3400 cm$^{-1}$, which belonged to the adsorbed water. No other peaks were observed in the SQD spectrum, which proved that there was no chemical reaction between the SQDs and PEG-400.[30] XPS was used to analyze the elements in the synthesized SQDs, as shown in Fig. 1C. The spectrogram results showed that all the expected elements were present, including C, O, and S. Fig. 1D shows the XPS spectrum of the S 2p electrons in the SQDs. Five peaks could be identified in the high-resolution XPS spectrum of S. The peaks located at 162.3 and 163.2 eV were attributed to elemental sulfur and peaks at the binding energies of 166.5, 168.2, and 169.3 eV could be assigned to $SO_3^{2-}$ ($2p_{2/3}$), $SO_3^{2-}$ ($2p_{2/3}$) or $SO_2^{2-}$ ($2p_{1/2}$), and $SO_3^{2-}$ ($2p_{1/2}$), respectively.[30] This result indicated that abundant sulfite groups were adsorbed on the surface of the synthesized SQDs, thus showing that SQDs with smaller volumes and larger specific surface areas were successfully prepared. The UV-vis absorption spectra shown in Fig. S1A(a)† were used to determine the characteristic absorption bands of the synthesized materials. The absorption bands corresponding to the SQDs were located at 303 nm. The weak absorption bands at 303 nm became increasingly prominent with the addition of $S_2^{2-}$.[30] Compared with the work by Shen and co-workers,[29] a certain blueshift was observed, which should be caused by $H_2O_2$ etching on the surface. The fluorescence properties of the SQDs are shown in Fig. S1A.† Under UV light with a wavelength of 365 nm, SQDs emitted blue-green light (inset). As shown in Fig. S1A(b),† when the fixed excitation wavelength was 365 nm, the emission wavelength of the SQDs appeared near 430 nm. It can be roughly seen from Fig. S1B† that the ECL intensity of the SQDs was significantly enhanced after the electrode was modified with SQDs, which proved that the ECL performance of the SQDs was excellent.

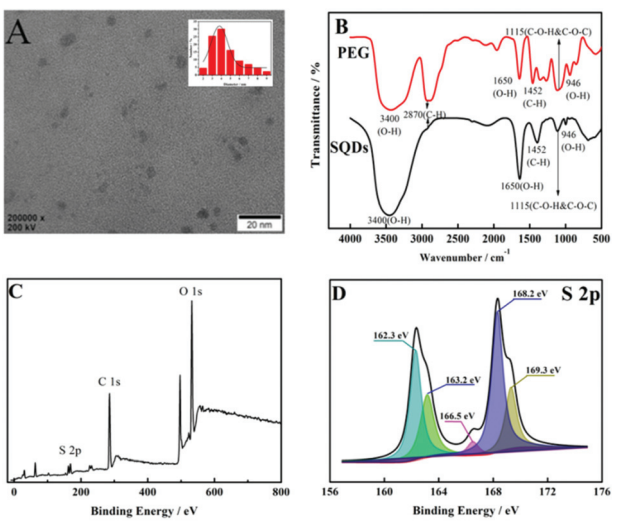


Fig. 1 (A) HR-TEM images of the pure SQDs with the diameter distribution of the SQDs (inset). (B) FT-IR spectra of the SQDs and pure PEG-400. (C) XPS spectra of the SQDs and (D) the S 2p region.

### Optimization of the experimental conditions

The pH of the co-reactant significantly influenced the ECL of the SQD electrode. Therefore, the pH of the $K_2S_2O_8$ co-reactant was optimized, and the result is shown in Fig. S2A.† As the pH of the $K_2S_2O_8$ co-reactant increased from 4 to 11, the ECL intensity initially increased and then decreased. The ECL intensity had a maximum value at a $K_2S_2O_8$ co-reactant pH of 7.4; therefore, this value was chosen as the optimal detection condition in this study. The other conditions were as follows: the scanning potential was −1.0 to 0 V, the scan speed was 100 mV s$^{-1}$, and the strength of the photomultiplier tube was

750 V. The ECL intensity of the electrode modified with the SQDs was measured under the action of a filter with a wavelength of 420–640 nm, and the results are shown in Fig. S2B.† The results show that the maximum emission wavelength of the ECL emission peak was approximately 450 nm, which was consistent with the results of the fluorescence spectrum analysis.

### ECL performance of the SQDs in the co-reactant

The possible ECL mechanism of the SQDs can be described as follows. First, when NADH was not present in the reaction, the SQDs could directly obtain electrons from the electrode to form $S^{\bullet-}$ (eqn (1)).[31] At the same time, $S_2O_8^{2-}$ was reduced to $SO_4^{\bullet-}$ and $SO_4^{2-}$ (eqn (2)).[32] Since the oxidation potential of $SO_4^{\bullet-}$ was very strong, the reaction of $SO_4^{\bullet-}$ and $S^{\bullet-}$ can turn $S^{\bullet-}$ into an excited state S* (eqn (3)).[33] The ECL signal was emitted when the excited state S* transition returned to the ground state (eqn (4)).[33] When NADH was present in the co-reactant, it reacted with $SO_4^{\bullet-}$ produced in eqn (2) (eqn (5)), resulting in less $SO_4^{\bullet-}$ produced with $S^{\bullet-}$, and therefore resulted in lower S* production. This will cause the quenching of the SQD ECL signals. The equations were as follows:

$$S + e^- \rightarrow S^{\bullet-} \quad (1)$$

$$S_2O_8^{2-} + e^- \rightarrow SO_4^{\bullet-} + SO_4^{2-} \quad (2)$$

$$S^{\bullet-} + SO_4^{\bullet-} \rightarrow S^* + SO_4^{2-} \quad (3)$$

$$S^* \rightarrow S + h\nu \quad (4)$$

$$NADH + SO_4^{\bullet-} \rightarrow NAD^+ + SO_4^{2-} \quad (5)$$

To verify our proposed mechanism, cyclic voltammetry was used, and the result is shown in Fig. S3.† With the addition of NADH, a significant shift to the right was clearly observed, as shown in Fig. S3A,† which was consistent with the mechanism we proposed. Fig. S3A† shows that when NADH existed, there would be a competition between $S^{\bullet-}$ and NADH, which would increase the consumption of $SO_4^{\bullet-}$ and promote further decomposition of $S_2O_8^{2-}$ (eqn (2)). Therefore, in the presence of NADH, the potential shifted significantly to the right, which was consistent with what we proposed. Fig. S3B† shows the control CVs of the bare GCE with NADH in $K_2S_2O_8$ solution. Compared with Fig. S3A,† it was obvious that there is no obvious interaction between the bare GCE and NADH. When the GCE modified the SQDs, there was a potential shift to the right and the current was significantly enhanced, indicating that SQDs had good conductivity and could accelerate electron transfer on the electrode surface.

### Linearity of the ECL sensor for NADH detection

In view of the importance of NADH in the biological sample and the phenomenon that NADH could reduce the SQDs/GCE, we added different concentrations of NADH (1 pM to 10 μM) to the co-reactant. The results are shown in Fig. 2A. Under the same conditions, we obtained a standard curve for the quantitative determination of NADH. According to the ECL intensity

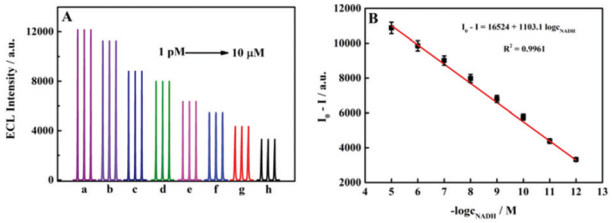


Fig. 2 (A) SQDs/GCE sensor with the addition of different concentrations of NADH solution. (B) Plot of the ECL intensity of the SQDs as a function of the concentration of NADH.

difference, the corresponding standard curve could be prepared, as shown in Fig. 2B. There was a certain linear relationship between $\Delta I$ and the logarithm of NADH concentration ($\Delta I = I_0 - I$, where $I_0$ represents the initial ECL intensity, and $I$ represents the ECL intensity after adding NADH). The regression equation was $I_0 - I = 16\,524 + 1103.1 \log c_{NADH}$ in the working concentration range from 1 pM to 10 μM with a limit of detection (LOD) of 1 pM. Table S1† summarizes the performance of some current NADH analysis methods. Compared with other methods, this sensor platform had a shoulder-width detection range and higher sensitivity. This result basically met the needs of actual sample determination.

### Linearity of the ECL sensor for the TBC detection

Theoretically, the TBC is positively correlated with the intracellular NADH content, therefore, NADH can be used as an important indicator for measuring the TBC. Therefore, in theory, a higher number of bacteria should correspond to a stronger degree of ECL quenching of the sensor. *E. coli* with a bacterial concentration of $10^3$–$10^7$ CFU $mL^{-1}$ was selected for the experiment, and the results are shown in Fig. 3A. The bacterial concentration and the degree of quenching showed a good linear relationship, and the linear equation was $I_0 - I = 1138.4 \log c_{E.\ coli} - 439.96$, $R^2 = 0.9927$ (Fig. 3B).

### Selectivity, stability and reproducibility of the ECL sensor

To further verify whether the proposed sensor has good selectivity for NADH, some common substances (urea, AA, UA, glucose and DA) were selected as interfering substances for the selectivity test, and the results are shown in Fig. 4. It can be obviously seen that the quenching of the ECL intensity of

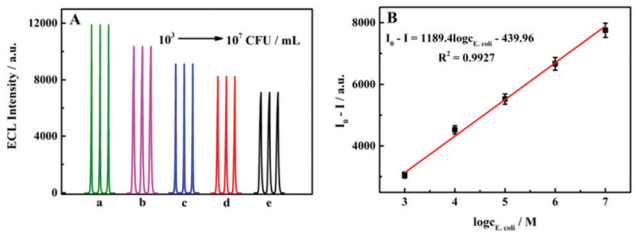


Fig. 3 (A) Response of the sensor when adding different concentrations of the TBC. (B) Plot of the ECL intensity of the TBC.

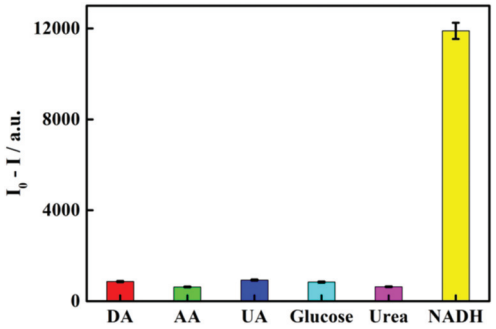


Fig. 4 Selectivity of other interfering substances against NADH: DA, AA, UA, glucose, urea and NADH.

the sensor by other interfering substances is far less than NADH. Combined with the experimental phenomenon, it is fully revealed that the constructed ECL sensor based on SQDs has a good selectivity for NADH recognition.

In addition, Fig. S4A† shows that SQDs generated strong and stable ECL signals. Fig. S4B† shows the reproducibility of the sensor. After the surfaces of five different GCEs were modified with SQDs, ECL measurements were performed under the same conditions. The results are shown in Fig. S4B.† After combining the SQDs with different GCEs, the ECL intensity was stable, and the reproducibility was good. Almost no difference in the ECL intensity was observed on the different electrodes. The stability is shown in Fig. S4C.† The synthesized SQDs were tested once a week under the same conditions for five weeks. Although the luminous intensity of the SQDs decreased slightly after 5 weeks, the experiment proved that the stability of the SQDs was good. During the test, SQDs was stored at 4 °C, away from light.

### Determination results of real samples

The determination results for various real biological samples are shown in Table 1. Under the conditions of the labeling experiment, the TBC recovery of tap water and mouse serum was 96.68–104.5% and 95.84–105.3%, respectively, with relative standard deviation (RSD) of 1.8–4.6% and 2.9–4.2%, respectively. However, in the real environmental samples, different TBCs were detected in samples from different areas. The results in Table 2 are similar to the standard method results. The experimental data fully showed that the ultrasensitive NADH-ECL sensor based on sulfur quantum dots exhibited good performance in detecting the TBC. Among the real samples, bacteria were not obviously seen in the tap water and mouse serum, while a certain number of bacteria were observed in the river water and lake water, which had a TBC of approximately $10^4$–$10^6$ CFU mL$^{-1}$.

Table 1 Determination of the TBC in real samples ($n$ = 3)

| Samples | Added, CFU mL$^{-1}$ | Found, CFU mL$^{-1}$ | Recovery (%) | RSD (%) |
|---|---|---|---|---|
| Tap water | $10^3$ | $9.668 \times 10^2$ | 96.68 | 4.6 |
| | $10^5$ | $1.045 \times 10^5$ | 104.5 | 3.8 |
| | $10^7$ | $9.871 \times 10^6$ | 98.71 | 1.8 |
| Mouse serum | $10^3$ | $1.012 \times 10^3$ | 101.2 | 3.1 |
| | $10^5$ | $9.584 \times 10^4$ | 95.84 | 2.9 |
| | $10^7$ | $1.053 \times 10^7$ | 105.3 | 4.2 |

Table 2 Determination of the TBC in real environmental samples with a check by the standard method ($n$ = 3)

| Samples | Times | ECL sensor, CFU mL$^{-1}$ | PCM, CFU mL$^{-1}$ |
|---|---|---|---|
| Lake water | 1 | $10^4$ | $10^4$ |
| | 2 | $10^4$ | $10^4$ |
| | 3 | $10^4$ | $10^4$ |
| River water | 1 | $10^4$ | $10^4$ |
| | 2 | $10^4$ | $10^4$ |
| | 3 | $10^6$ | $10^6$ |

## Conclusions

In this study, a novel sensitive and simple ECL sensor was established for detecting TBC based on SQDs synthesized *via* a top-down approach. The morphological characteristics and ECL performance of the SQDs were extensively researched, and an application based on this ECL sensor could detect the TBC by detecting NADH, which has great significance to the environment and human society. The ECL sensor had a detection range of 1 pM to 10 μM, and the LOD was 1 pM. An ECL sensor was used to detect the TBC in nearby water (tap water, lake water and river water), and the pollution of the water was roughly evaluated based on the experimental results. In addition, mouse serum was also selected as a real biological sample. This study provided a new and convenient method of detecting the total number of bacteria, which is of great significance for improving people's quality of life and controlling environmental pollution.

## Conflicts of interest

There are no conflicts of interest to declare.

## Acknowledgements

The authors gratefully acknowledge the support from the National Natural Science Foundation of China (21778047) and the Natural Science Foundation of Shandong Province (grant no. ZR2021MB024).

## Notes and references

1 K. W. Lien, M. X. Yang and M. P. Ling, *Microorganisms*, 2020, **8**, 676.
2 Z. Zhu, X. Zhu, F. Kong and W. Guo, *J. Dairy Sci.*, 2019, **102**, 7895–7903.

3 J. Zurita, F. Yánez, G. Sevillano, D. O. Paredes and A. P. Y. Mio, *Lett. Appl. Microbiol.*, 2020, **70**, 203–209.
4 N. Fegan and K. S. Gobius, *Curr. Top. Microbiol.*, 2013, **366**, 49–62.
5 X. Hu, M. Wang, Y. Pan, Y. Xie and S. Yu, *Front. Vet. Sci.*, 2020, **7**, 201.
6 J. H. Lee, S. C. Regmi, J. A. Kim, M. H. Cho, H. Yun, C. S. Lee and J. Lee, *Infect. Immun.*, 2011, **79**, 4819–4827.
7 C. H. Gayathri, P. Mayuri, K. Sankaran and A. S. Kumar, *Biosens. Bioelectron.*, 2016, **82**, 71–77.
8 J. P. Gorsuch, Z. Jones, D. L. Saint and C. L. Kitts, *J. Microbiol. Methods*, 2019, **164**, 105682.
9 F. Yu, Y. Li, M. Y. Li, L. H. Tang and J. J. He, *Biosens. Bioelectron.*, 2017, **89**, 880–885.
10 G. Macori, S. C. McCarthy, C. M. Burgess, S. Fanning and G. Duffy, *J. Microbiol. Methods*, 2019, **165**, 105703.
11 P. Zhang, L. L. Zhuang, D. Zhang, J. X. Xu, X. H. Dou, C. M. Wang and J. S. Gong, *Foodborne Pathog. Dis.*, 2018, **15**, 776–781.
12 A. Mortari and L. Lorenzelli, *Biosens. Bioelectron.*, 2014, **60**, 8–21.
13 A. A. Burkin, G. P. Kononenko, G. A. Kochkina and S. M. Ozerskaia, *Appl. Biochem. Microbiol.*, 2007, **43**, 453–458.
14 T. S. Blacker and M. R. Duchen, *Free Radicals Biol. Med.*, 2016, **100**, 53–65.
15 J. Mach, A. W. Midgley, S. Dank, R. S. Grant and D. J. Bentley, *Nutrients*, 2010, **2**, 319–329.
16 F. Marchetti, M. Cainzos, S. Shevtsov, J. P. Cordoba, L. D. Sultan, A. Brennicke, M. Takenaka, G. Pagnussatl, B. O. Ostersetzer and E. Zabaleta, *Plant Cell Physiol.*, 2020, **61**, 1080–1094.
17 M. A. Fomin, R. I. Dmitriev, J. Jenkins, D. B. Papkovsky, D. Heindl and B. König, *ACS Sens.*, 2016, **1**, 702–709.
18 P. Sun, H. Zhang, Y. Sun and J. Liu, *Spectrochim. Acta, Part A*, 2020, **245**, 118919.
19 D. Compagnone, C. J. Mcneil, D. Athey, C. D. Ilio and G. G. Guilbault, *Enzyme Microb. Technol.*, 1995, **17**, 472–476.
20 X. H. Liu, Y. Xu and I. Mpc, *Anal. Chem.*, 1995, **67**, 3211.
21 F. S. Omar, N. Duraisamy, K. Ramesh and S. Ramesh, *Biosens. Bioelectron.*, 2016, **79**, 763–755.
22 P. Stufano, A. R. Paris and A. Bocarsly, *ChemElectroChem*, 2017, **4**, 1066–1073.
23 K. Yamada, N. Hara, T. Shibata, H. Osago and M. Tsuchiya, *Anal. Biochem.*, 2006, **352**, 282–285.
24 K. Potrykus, N. E. Thomas, B. B. Olszewska, M. Sobala, M. Dylewski, T. James and M. Cashel, *Front. Microbiol.*, 2020, **11**, 581271.
25 J. R. Zhang, J. Chen and Z. M. Liu, *J. Anal. Chem.*, 2010, **38**, 1219–1226.
26 F. Zhang, H. Chen, P. G. He and Y. Z. Fang, *J. Anal. Chem.*, 2013, **41**, 1–9.
27 K. Yi and C. Wei, *Int. J. Electrochem. Sci.*, 2017, **12**, 3472–3482.
28 A. J. Stewart, E. O'Reilly, R. D. Moriarty, P. Bertoncello, T. E. Keyes, R. J. Forster and L. Dennany, *Electrochim. Acta*, 2015, **157**, 8–14.
29 L. H. Shen, N. W. Hong, S. N. Liu, Z. W. Bai and S. C. Zhang, *J. Am. Chem. Soc.*, 2018, **140**, 7878–7884.
30 Z. G. Wang, H. G. Wang, Y. Xiong, S. V. Kershaw, T. Z. Li, Y. Wang and A. L. Rogach, *Angew. Chem., Int. Ed.*, 2019, **58**, 7040–7044.
31 R. Z. Zhang, J. R. Adsetts, Y. T. Nie, X. H. Sun and Z. F. Ding, *Carbon*, 2017, **129**, 45–53.
32 H. P. Huang, J. J. Li and J. J. Zhu, *Anal. Methods*, 2011, **3**, 33–42.
33 K. L. Ji, Y. F. Wang, L. B. Mao, Y. Z. Wang and X. H. Zhang, *Sens. Actuators, B*, 2021, **345**, 130405.